Linearly rising soliton trajectories*

Shu-Yuan Chu and Peter Kaus
Department of Physics, University of California, Riverside, California 92502
(Received 4 October 1976)

Linearly rising soliton trajectories without parity partners are obtained from the nonlinear field equations of a Dirac field in four dimensions with universal Fermi self-interaction. The model is Lorentz and global-gauge invariant.

I. INTRODUCTION

It has been known for a long time[1] that nonlinear field equations of Lagrangian field theory possess localized solutions with particlelike properties at the classical level. These particlelike solutions, solitons or solitary waves, have received renewed interest recently,[2] which stems from the expectation that these soliton solutions will also emerge in quantum chromodynamics (QCD) and may be the key to the understanding of quark confinement and the spectrum of the composite and extended hadrons.

In this paper we take the first step to study Regge trajectories in relativistic field theories through such soliton solutions. As a preparation for the full complexity of QCD, which we hope to examine in the future, we consider the nonlinear field equations in four dimensions of a Dirac field with universal Fermi self-interaction. These calculations should be considered mainly methodological, since this model is much simpler than QCD. However, it is fully relativistic, global-gauge (but not local-gauge) invariant, and readily adaptable to incorporate color symmetry. The MacDowell symmetry is satisfied, so that the model can address the question of parity partners. The "Regge trajectories" for this nonlinear spinor field for strong self-coupling will turn out to be linear in $s = E^2$ without parity doubling.

The plan of the rest of the paper is as follows. In Sec. II we write down the nonlinear spinor field equations. By comparing with the results of an earlier paper,[3] we establish the MacDowell symmetry and explain why linearly rising Regge trajectories are expected. In Sec. III we obtain numerical soliton solutions with definite angular momentum. The leading rising soliton trajectories of both parities are displayed as well as the first daughter trajectories, especially in the limit of strong coupling and deep binding. We discuss the features of the soliton solutions which will be used in Sec. IV to construct approximate solutions in closed form for deep binding and large angular momentum. Section V contains some concluding remarks.

II. NONLINEAR FIELD AS A RELATIVISTIC MODEL FOR SOLITON TRAJECTORIES

Consider the Lagrangian density of a Dirac field with universal Fermi self-interaction[4]:

$$\mathcal{L} = -\tfrac{1}{2}(\bar{\Psi}\gamma_\mu \partial_\mu \Psi - \partial_\mu \bar{\Psi}\gamma_\mu \Psi) - \mu\bar{\Psi}\Psi + \mathcal{L}_I , \tag{2.1}$$

$$\mathcal{L}_I = \sum_{\sigma=1}^{5} C_\sigma (\bar{\Psi}\Gamma_\rho^\sigma \Psi)(\bar{\Psi}\Gamma_\rho^\sigma \Psi)$$

where μ is the bare mass, C_σ are the coupling constants for the invariants S, V, T, A, P, and Γ_ρ^σ are the corresponding Dirac matrices. With the introduction of the color degrees of freedom the problem of color-singlet states formed from three quarks reduces to solving the nonlinear field equations for a single quark field, because all three quarks can have the same wave function. The only change is that the coupling constant is changed by a factor $N = 3$.[5] With all four spinors in $\mathcal{L}_I$ identical, the most general form of $\mathcal{L}_I$ is

$$\mathcal{L}_I = \gamma_S(\bar{\Psi}\Psi)^2 + \gamma_P(\bar{\Psi}\gamma_5\Psi)^2 , \tag{2.2}$$

with

$$\gamma_S = C_S + C_V + C_T + C_A ,$$

$$\gamma_P = C_P - C_V + C_T - C_A .$$

The Euler-Lagrange equations of the Lagrangian density (2.1) are in general not separable. We therefore look for solutions of the variational equation

$$\delta \int \mathcal{L}\, d^4x = 0 \tag{2.3}$$

within a class of variational functions of the form

$$\Psi_\pm = \tfrac{1}{2}[F(r)(1+\gamma_4)\Omega_\pm + iG(r)(1-\gamma_4)\Omega_\pm]e^{i\omega t} , \tag{2.4}$$

where $\Omega_\pm$ are eigenfunctions of the operator

$$\hat{\kappa} = \gamma_4[-i\vec{\sigma}\cdot(\vec{r}\times\vec{\nabla}) + 1] \tag{2.5}$$

with eigenvalues $\kappa = \pm(j+\frac{1}{2})$, $\kappa > 0$, and $\kappa < 0$ corresponding to states of opposite parity. Substituting the comparison functions (2.4) into the Lagrangian density (2.1) and performing the variation (2.3), the angular functions $\Omega_\pm$ are fixed and only the

radial functions F and G are to be varied independently. We obtain

$$\frac{dF}{dr}+\frac{1-\kappa}{r}F+(\mu-\omega)G+[2\gamma_S d_S(\kappa)(G^2-F^2)-4\gamma_P d_P(\kappa)F^2]G=0\,, \tag{2.6}$$

$$\frac{dG}{dr}+\frac{1+\kappa}{r}G+(\mu+\omega)F-[2\gamma_S d_S(\kappa)(F^2-G^2)-4\gamma_P d_P(\kappa)G^2]F=0\,.$$

Here $d_{S,P}(\kappa)$ are the results of the integration over angles and are given by

$$d_S(\kappa)=\int_0^{\pi}\int_0^{2\pi}\left|Y^{|\kappa|-1}_{|\kappa|-1}\right|^4\sin\theta\,d\theta\,d\phi=\frac{1}{2\pi^{3/2}}\frac{\Gamma^2(\kappa+\frac{1}{2})\Gamma(2\kappa-1)}{\Gamma^2(\kappa)\Gamma(2\kappa-\frac{1}{2})} \tag{2.7}$$

and

$$d_P(\kappa)=\int_0^{\pi}\int_0^{2\pi}\left|Y^{|\kappa|-1}_{|\kappa|-1}\right|^4\cos^2\theta\sin\theta\,d\theta\,d\phi=\frac{1}{4\pi^{3/2}}\frac{\Gamma^2(\kappa+\frac{1}{2})\Gamma(2\kappa-1)}{\Gamma^2(\kappa)\Gamma(2\kappa+\frac{1}{2})}=\frac{1}{4\kappa-1}d_S(\kappa)\,.$$

We note that as $|\kappa|=j+\frac{1}{2}$ becomes greater than unity $d_S(\kappa)$ rapidly approaches $\sqrt{\kappa}/(2\pi)^{3/2}$ and $d_P(\kappa)\to 1/4(2\pi)^{3/2}\sqrt{\kappa}$.

The invariance of the Lagrangian implies the following conserved quantities:

$$Q=\int\Psi^*\Psi\,d^3x\,,$$

$$M=\int\mathcal{L}\,d^3x=\tfrac{1}{2}[\Psi^*\partial_4\Psi-(\partial_4\Psi^*)\Psi]\,d^3x\,, \tag{2.8}$$

$$j_z=\int\Psi^*\left(-i\frac{\partial}{\partial\phi}+\tfrac{1}{2}\sigma_z\right)\Psi\,d^3x\,.$$

Localized solutions of Eq. (2.6) are interpreted as particles of mass M and angular momentum j_z.

The MacDowell symmetry equates partial-wave S-matrix elements of opposite parity: $S_+(j,-E)=S_-(j,E)$, when E is the total energy. In a previous paper we have discussed the MacDowell symmetry in the context of the Dirac equation with a confining "scalar" potential. We find that the MacDowell symmetry can be expressed as relations between opposite-parity solutions of the Dirac equation. In the present relativistic model the total energy M for solutions of (2.6) is given by

$$M=\int[\gamma_S d_S(\kappa)(G^2-F^2)^2-4\gamma_P d_P(\kappa)F^2G^2]r^2dr+\omega\int(F^2+G^2)r^2dr\,. \tag{2.9}$$

Hence the continuation of $M\to -M$ corresponds to $\gamma_S\to-\gamma_S$, $\gamma_P\to-\gamma_P$, and $\omega\to-\omega$. From (2.6) we see that the MacDowell symmetry is explicitly satisifed. To every positive-parity solution $\kappa=j+\frac{1}{2}$ there corresponds a negative-parity solution $\kappa=-(j+\frac{1}{2})$ with $M\to -M$; specifically,

$$F_+(j,-M)=G_-(j,M)\,,\qquad G_+(j,-M)=F_-(j,M)\,. \tag{2.10}$$

Equation (2.6) can be scaled to dimensionless form:

$$\frac{df}{dx}+\frac{1-\kappa}{x}f+(1+\beta)g+\left(g^2+\frac{\lambda}{2}f^2\right)g=0\,,$$

$$\frac{dg}{dx}+\frac{1+\kappa}{x}g+(1-\beta)f-\left(f^2+\frac{\lambda}{2}g^2\right)f=0\,. \tag{2.11}$$

This is the result of making the following substitutions:

$$r=x/\mu\,,\qquad \omega=-\mu\beta\,,\qquad F(r)=[\mu/2\gamma_S d_S(\kappa)]^{1/2}f(x)\,,\qquad G(r)=[\mu/2\gamma_S d_S(\kappa)]^{1/2}g(x)\,, \tag{2.12}$$

and

$$\lambda=-\left[2+4\left(\frac{\gamma_P}{\gamma_S}\right)\left(\frac{1}{4|\kappa|-1}\right)\right].$$

We then have for the angular momentum, mass, and coupling constant, γ_S, in terms of $f(x)$ and $g(x)$,

$$j_z=|\kappa|-\tfrac{1}{2}\,,\qquad M=\mu(\beta+I_2/I_1)\,,\qquad \gamma_S=I_1/2\mu^2 d_S(\kappa)\,, \tag{2.13}$$

where

$$I_1=\int(f^2+g^2)x^2dx\,,\qquad I_2=\int(f^4+\lambda f^2g^2+g^4)x^2dx\,.$$

In Ref. 3 we also find that in order for the trajectory to be linear in $s=M^2$, the potential $V(r)$ should have a $\sqrt{j}$ dependence. It is interesting to note that the effective scalar coupling in (2.6), namely $\gamma_S d_S(\kappa)$, will indeed have this behavior, since

$$d_S(\kappa)\to\frac{|j+\frac{1}{2}|^{1/2}}{(2\pi)^{3/2}}\,,\qquad |\kappa|=|j+\tfrac{1}{2}|\gg 1\,.$$

We therefore expect the Regge trajectories to be linear in $s=M^2$, at least for large angular momentum. For large κ the pseudoscalar coupling

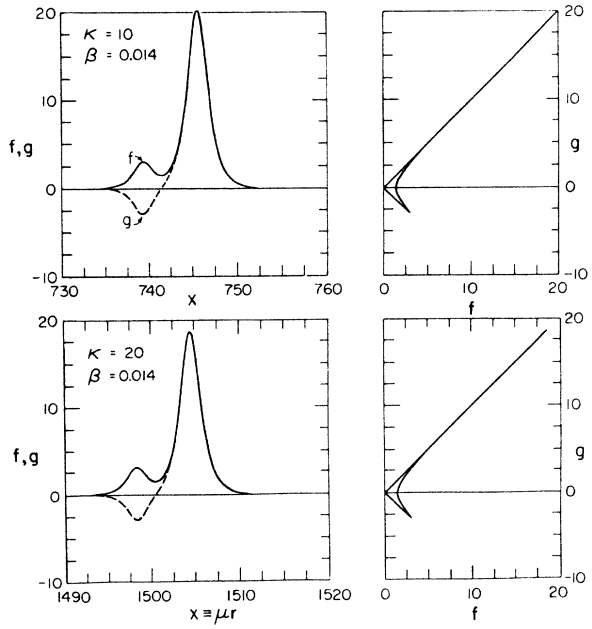

FIG. 1. Typical solutions of the radial equation. Plotted are $f(x)$ (——) and $g(x)$ (---) vs $x \equiv \mu r$. The right panels give f vs g. The upper panels correspond to $\kappa \equiv j + \frac{1}{2} = 10$; the lower panels correspond to $\kappa = 20$. The energy parameter $\beta \equiv -\omega/\mu = 0.014$ for both cases.

$$\frac{\gamma_P d_P(\kappa)}{\gamma_S d_S(\kappa)} \to \frac{\gamma_P/\gamma_S}{4|\kappa|} \to 0$$

because of (2.7). Thus, unless γ_S actually vanishes, the effective coupling is always scalar for large spins and we expect the linear behavior of these c-number Regge trajectories to assert itself. The scalar case, $\gamma_P = 0$ or $\lambda = -2$, also has the property that the variational ansatz (2.4) actually "separates" the Lagrangian for the case $|\kappa| = 1$, and the differential equations (2.11) may then be considered exact.[1]

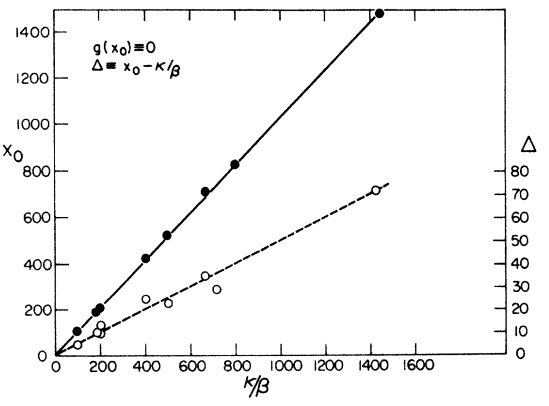

FIG. 2. The zero of g, i.e., x_0 (—●—), and the quantity $\Delta \equiv x_0 - \kappa/\beta$, (---○---), as functions of κ/β, for a random selection of solutions with various (large) κ and various (small) β. Note that Δ is around 5% of x_0 for these solutions.

For these reasons we have chosen $\gamma_P = 0$ and $\lambda = -2$ for the investigations in this paper. We also note that the ansatz (2.4) is, of course, exact for the free Dirac equation. For states with the higher angular momentum, the mass, M, of the soliton solution approaches the bare mass, μ. The solutions resemble increasingly the free solutions, and the nonlinear term becomes less dominant. We then expect, heuristically, that the solutions of (2.11), based on the variational ansatz (2.4), become "good" solutions with increasing spin.

III. NUMERICAL SOLUTIONS

The scaled equations for f and g with $\lambda = -2$ and $\gamma_P = 0$ are then

$$\frac{df}{dx} + \frac{1-\kappa}{x} f + (1+\beta)g + (g^2 - f^2)g = 0\,,$$
$$\frac{dg}{dx} + \frac{1+\kappa}{x} g + (1-\beta)f + (g^2 - f^2)f = 0\,. \tag{3.1}$$

This is just the radial Dirac equation with a scalar "potential," $V(x)$, given by $-(f^2 - g^2)$. In this section we discuss various features of the numerical solutions which lead to linearly rising trajectories.

In Fig. 1 we show f and g as functions of x and f vs g, for a typical small β (deep binding), for two values of $\kappa = j + \frac{1}{2}$. We notice that there are two peaks, both occurring very close to x_0, which is defined by $g(x_0) = 0$. From the f vs g "phase" plot, we see clearly that near each peak the magnitudes of f and g are very nearly equal. The difference,

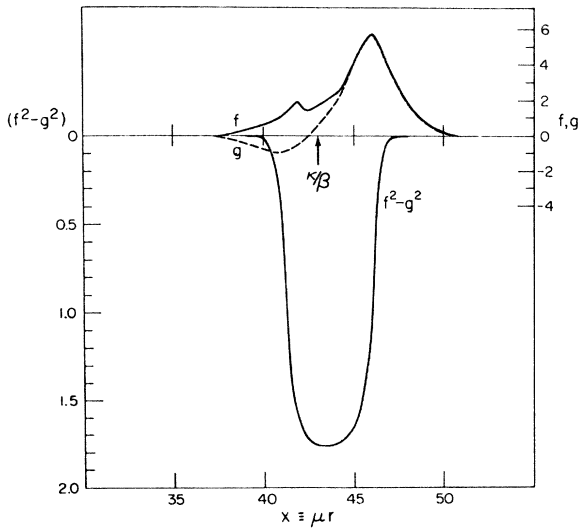

FIG. 3. The self-consistent "well," $-(f^2 - g^2)$, and the solutions f, g as functions of the dimensionless radius $x \equiv \mu r$. The case shown here is $\kappa = j + \frac{1}{2} = 4$ and $\beta = -\omega/\mu = 0.093$.

however, is important. In Fig. 2, we plot $-(f^2-g^2)$ as a function of x. It is seen to be a narrow well of depth of order 2 near the radius x_0. The important difference between a self-consistent and a potential well is that the former's position moves with the spin quantum number κ as well as the energy parameter β. The depth and width of the well, however, are essentially independent of these parameters.

Since the solutions in question here are very localized in $x=\mu r$, we may consider x_0, defined by $g(x_0)=0$, as the radius of the solution. Figure 3 shows x_0 as a function of κ/β for eight random solutions. The quantity $\Delta \equiv x_0 - \kappa/\beta$ is also shown. That $\kappa \propto x_0\beta$ is not really surprising, once the extreme radial localization is established. In dimensional units it means that $j \propto \langle r\rangle \omega\hbar$, and with $\omega \propto Mc/\hbar$ we have $j \propto \langle r\rangle Mc$. Considering that in the region of localization $f \approx g$, which implies $v \approx c$, then we see that the relationship in question, i.e., $\kappa \propto x_0\beta$, only expresses the fact that we have a thin ring of mass $-\omega$, rotating with a "velocity" near c to produce an angular momentum j. However, that the *equality* $\kappa = x_0\beta$ seems so closely satisfied ($\Delta \equiv x_0 - \kappa/\beta$ is only around 5% of κ/β for the solutions tested) is considerably more obscure. After all, $\beta\mu \equiv -\omega$, the rotating mass, is not *equal* to the mass, and the contribution from the nonlinear part, $(I_2/I_1)\mu$ in (2.11), is not negligible. In fact, for large κ and small β we have $\beta\mu \approx (I_2/I_1)\mu$, that is, the total mass of the soliton is shared equally by the "particle" itself and the "potential." This is reminiscent of a virial theorem, but we do not claim to understand it. The high degree of localization of the solutions, which is another ingredient of the $\kappa = x_0\beta$ argument, is much better understood and will be discussed in the next section. We also observed that $f_{\max}$ is linearly proportional to $1/\sqrt{\beta}$.

In order to interpret these numerical soliton solutions of the scaled equations (3.1), we repeat what the mass and (scalar) coupling is in terms of the solutions f and g. With the definitions

$$I_1 \equiv \int (f^2+g^2)x^2\,dx$$

and (3.2)

$$I_2 \equiv \int (f^2-g^2)^2x^2\,dx$$

we have

$$M/\mu = \beta + I_2/I_1 \tag{3.3}$$

and

$$\gamma\mu^2 = I_1/2d_S(\kappa) \tag{3.4}$$

(we drop the subscript of γ_S since $\gamma_P=0$).

The equations (3.1) were integrated numerically for various (positive and negative) values of κ and in each case for a variety of β, under the boundary conditions at the origin and infinity which make the integrals I_1 and I_2 finite. The coupling $\gamma\mu^2$ and the mass M/μ were obtained for the solutions after the fact. In other words, in order to get Regge trajectories corresponding to one theory (one coupling γ), interpolation from the runs actually obtained was used.

We now combine the features that $f_{\max} \propto 1/\sqrt{\beta}$ and $x_0 \propto \kappa/\beta$ and the fact that the localization of the solutions is practically constant. We have from (3.2) and Figs. 2 and 3

$$I_1 \propto (1/\beta)(\kappa/\beta)^2 \tag{3.5}$$

and

$$I_2 \propto (\kappa/\beta)^2$$

and from (3.4)

$$I_1 = 2\gamma\mu^2 d_S(\kappa) \propto \sqrt{\kappa}\,, \tag{3.6}$$

since $d_S(\kappa)$ is proportional to $\sqrt{\kappa}$. We find then for solutions corresponding to the same γ that

$$\beta \propto \sqrt{\kappa}\,. \tag{3.7}$$

Solutions for one "theory," i.e., for the same γ, thus have the property

$$x_0 \approx \frac{\kappa}{\beta} \propto \kappa^{1/2}\,, \qquad f_{\max} \propto \frac{1}{\sqrt{\beta}} \propto \frac{1}{\kappa^{1/4}}\,. \tag{3.8}$$

We show in Fig. 4 numerical solutions for f and g

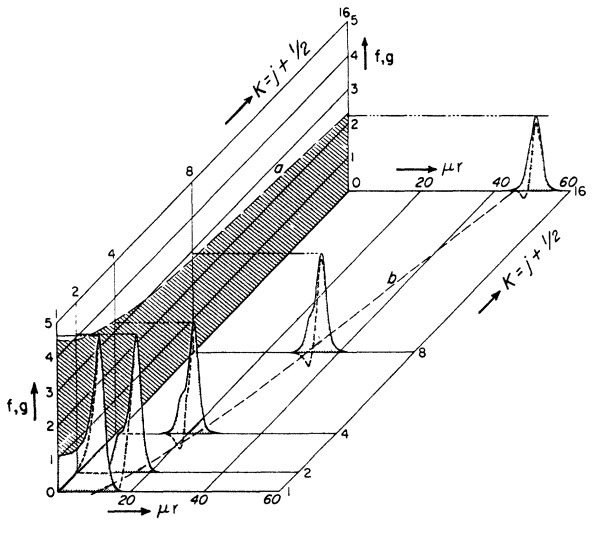

FIG. 4. Solutions f, g which correspond to the dimensionless coupling constant ($\gamma\mu^2=10^5$) for various $\kappa = j+\frac{1}{2}$ as functions of $x=\mu r$. The curves (a) $f = 4.7/\kappa^{1/4}$ and (b) $\mu r = 11\kappa^{1/2}$ are given for guidance. See text for significance of (a) and (b) as approximations for height and "radius" of solutions.

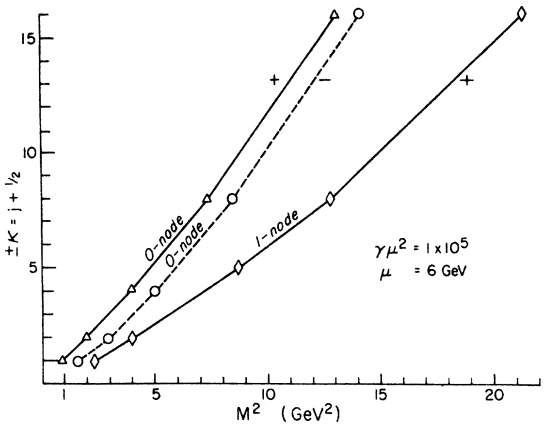

FIG. 5. Soliton Regge trajectories. Shown are the 0-node solutions for both parities (±) and the first daughter trajectory for + parity. The mass μ is not significant, but was chosen only to give the usual slope for the top trajectory for this particular coupling ($\gamma\mu^2 = 10^5$).

which correspond closely to one coupling constant, $\gamma\mu^2 = 10^5$, for $\kappa = j + \frac{1}{2}$ ranging from $\kappa = 1$ to $\kappa = 16$. Since these are actual numerical solutions of the scaled equations (3.1), they do not agree exactly with $\gamma\mu^2 = 10^5$, for the reasons discussed above following Eq. (3.4). However, all the solutions depicted give this coupling to within 5%. Curves corresponding to (a) $f = 4.7/\kappa^{1/4}$ and (b) $x = \mu r = 11\kappa^{1/2}$ are shown as a test of the relations (3.8). For these solutions β was taken very close to $0.09\sqrt{\kappa}$.

The linearity of the trajectories now follows. From (3.3) and (3.5)

$$M/\mu \approx \beta + I_2/I_1 \approx (1+C)\beta\,, \tag{3.9}$$

and from (3.7)

$$M/\mu \propto \sqrt{\kappa}$$

or

$$j = -\tfrac{1}{2} + \alpha' M^2\,. \tag{3.10}$$

Thus, the trajectories are expected to be linear. We have already discussed the fact that $C \approx 1$, or that the mass contribution to the soliton from the nonlinear part, i.e., $\mu(I_2/I_1)$, is about equal to the mass contribution from the energy parameter, i.e., $\mu\beta = -\omega$. This does not directly affect the linearity of the trajectories, as can be seen from (3.9), but it is a suggestive curiosity.

The features of the solutions discussed here [Eqs. (3.5)–(3.8)], which lead to linear trajectories, are not exact, of course. They hold in particular in the region where β is small and κ is large. These are seemingly contradictory demands, since they imply that M/μ should be both small and large. However, the stronger the coupling, $\gamma\mu^2$, the larger the range of spins, κ, for which β or M/μ is small. We therefore expect trajectories rising linearly to larger spin values the bigger we make $\gamma\mu^2$, corresponding to stronger binding.

The trajectories resulting from numerical integration are shown in Figs. 5 and 6. In both figures trajectories up to $\kappa = 16$ are shown, with the actually computed points indicated. The bare mass μ was chosen in each case, so as to produce the usual slope of $\alpha' \approx 1$ GeV^{-2} for small angular momenta. In Fig. 5 we see the top positive-parity trajectory, the top negative-parity trajectory, and the first positive-parity daughter. Note that for the coupling $\gamma\mu^2 = 10^5$ the trajectories start curving up at the higher κ values, but also note that for $\kappa = 16$ the ratio of soliton mass to bare mass for the top trajectory is of order $\frac{1}{2}$, which is not sufficiently bound for the arguments for linearity to hold. The negative-parity top trajectory has generally the same slope, but lags some $1\frac{1}{2}$ units of angular momentum behind. This trajectory cannot be construed to be an analytic continuation (or parity partner) of the top trajectory, a fact which is not surprising considering the $\sqrt{\kappa}$ nature of the effective coupling and the discussion of our previous paper.[3]

The straightening out of the trajectories for large coupling is demonstrated in Fig. 6. When $\gamma\mu^2$ is of order 10^7, the trajectories are linear at least up to $\kappa = 16$. Notice that in the $\gamma\mu^2 = 10^7$ case the soliton-to-bare-mass ratio for $\kappa = 16$ is only about 1/6, so that the soliton is still very deeply bound and the arguments for linearity apply.

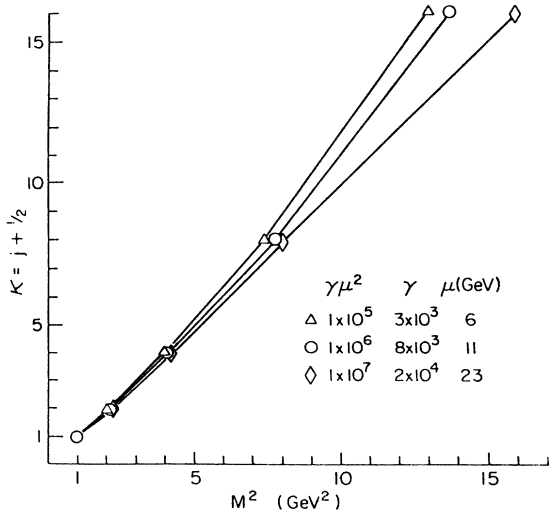

FIG. 6. The leading trajectory with the self-coupling γ as parameter. In each case the "mass" μ was chosen to give a slope of $\alpha' \approx 1$ GeV^{-2} for small spins.

IV. APPROXIMATE SOLUTIONS IN CLOSED FORM FOR DEEP BINDING AND LARGE ANGULAR MOMENTUM

The numerical solutions obtained in the preceeding section for deep binding (small β) and large angular momentum (large κ) have the important feature that f and g are appreciably different from zero only in a small range of x around x_0, the radius at which g vanishes. From Sec. III $x_0 \approx \kappa/\beta \gg 1$ in that regime. This feature allows us to construct approximate solutions in closed form characterized by κ, β, and x_0.

We begin by approximating the scaled differential equation (3.1) for f and g by

$$\begin{aligned} &\frac{df}{dx} - \frac{\kappa}{x_0} f + (1+\beta)g + (g^2 - f^2)g = 0 , \\ &\frac{dg}{dx} + \frac{\kappa}{x_0} g + (1-\beta)f + (g^2 - f^2)f = 0 , \end{aligned} \tag{4.1}$$

with the condition $g(x_0) = 0$. The error made in this approximation is of the order of $1/\kappa$ and $\Delta x/x_0$, where Δx is the range of x where f and g are appreciably different from zero.

Equation (4.1) can be put in the suggestive form[1]

$$\begin{aligned} \frac{df}{dx} &= -\frac{\partial H}{\partial g} , \\ \frac{dg}{dx} &= \frac{\partial H}{\partial f} , \end{aligned} \tag{4.2}$$

where

$$H = \frac{1}{2}\left[-\frac{2\kappa}{x_0} fg + (1+\beta)g^2 - (1-\beta)f^2 + \tfrac{1}{2}(f^2 - g^2)^2 \right] . \tag{4.3}$$

It follows that H is independent of x for a solution of Eq. (4.1). Solutions of (4.1) which are integrable must correspond to the $H = 0$ contour in the f-g "phase plane."

It is convenient for the present to define

$$\begin{aligned} J &= (f^2 - g^2) , \\ \theta &= \tanh^{-1}(g/f) . \end{aligned} \tag{4.4}$$

We have

$$H = \tfrac{1}{2}\left[-\frac{\kappa}{x_0} J \sinh 2\theta - (1 - \beta\cosh 2\theta)J + \tfrac{1}{2}J^2 \right] . \tag{4.5}$$

For $H = 0$, we express J in terms of θ:

$$\begin{aligned} J &= \frac{2\kappa}{x_0}\sinh 2\theta + 2(1 - \beta\cosh 2\theta) , \\ f^2 + g^2 &= J\cosh 2\theta \\ &= \left[\pm\frac{2\kappa}{x_0}(\cosh^2 2\theta - 1)^{1/2} - 2\beta\cosh 2\theta + 2 \right] \\ &\quad \times \cosh 2\theta . \end{aligned} \tag{4.6}$$

It is clear from (4.3) that the maximum $f^2 + g^2$ for $H = 0$ must occur when $f^2 \approx g^2$. This means that $\cosh^2\theta \approx \sinh^2\theta$ and $\theta = \tanh^{-1}(g/f)$ is large. In order to get a feeling for the nature of the solution of the approximate equation (4.1), we identify the maximum of the density $f^2 + g^2$:

$$f^2 + g^2 \approx 2\cosh 2\theta - 2\left(\beta \mp \frac{\kappa}{x_0}\right)\cosh^2 2\theta , \tag{4.7}$$

which clearly has a maximum when

$$2\cosh 2\theta = \frac{1}{\beta \mp \kappa/x_0} \tag{4.8}$$

at these two values:

$$f^2 + g^2 = \frac{\frac{1}{2}}{\beta \mp \kappa/x_0} = \begin{cases} 1/2\Delta' \\ 1/2(2\beta + \Delta') \approx \frac{1}{4}\beta , \end{cases} \tag{4.9}$$

where $\Delta' \equiv \beta - \kappa/x_0 = \Delta(\beta/x_0)$ (see Fig. 2). Since $\Delta' \equiv \beta - \kappa/x_0$, for κ positive, the larger ($\frac{1}{2}\Delta'$) peak occurs when $x > x_0$ ($\sinh 2\theta > 0$). For κ negative, $x < x_0$ ($\sinh 2\theta < 0$) gives the larger peak.

A good example of the two peaks is seen in Fig. 1. The ratio of the two peaks is seen to be about $\frac{20}{3}$. The square of this ratio is about 40. This, according to (4.9), should be equal to $2\beta/\Delta'$. Now in Fig. 2, we established the numerical fact that $\Delta' \approx 0.05\beta$ for all solutions, which also gives the ratio $2\beta/\Delta' \approx 40$. Furthermore, when $f \approx g$, $f_{\max} = 1/\sqrt{8\beta}$ from (4.9). For the cases of Fig. 1, $1/\sqrt{8\beta} = 3$, since $\beta = 0.14$ for these solutions. So we see that the solutions of (4.1), which are the full equations (3.1) with $(\kappa \pm 1)/x$ replaced by κ/x_0, are an excellent approximation to the solutions of the full equations (3.1), at least in the regime of small β and large κ. The important parameters in the solutions of (4.1) are seen to be β, κ, and $\Delta' \equiv \beta - \kappa/x_0$. Of course, in the full equations (3.1) β and κ are input, but x_0, defined by $g(x_0) = 0$, is output for integrable solutions. Therefore, Δ' is not a parameter in the full equation. The discussion in Sec. III makes it very plausible that $\beta \approx \kappa/x_0$ and that Δ' should be small and positive, since it is related to $1 - v/c$. What is not clear is how we might predict its numerical value ($\approx 0.05\beta$), and that is why we are treating Δ' as an independent (small) parameter in the approximate equations (4.1).

We finish this section by giving the explicit solution of (4.1), that is of f and g as functions of $x = \mu r$ with β and Δ' parameters.

From (4.2) and (4.3) we have (for $\kappa > 0$)

$$\begin{aligned} J = &[1 - \beta(\cosh 2\theta - \sinh 2\theta) - \Delta'\sinh 2\theta] \\ &+ \{[1 - \beta(\cosh 2\theta - \sinh 2\theta) - \Delta'\sinh 2\theta]^2 + 4H^2\}^{1/2} \end{aligned} \tag{4.10}$$

and

$$\frac{dJ}{dx} = -2\beta J(\sinh 2\theta - \cosh 2\theta) - 2\Delta' J \cosh 2\theta . \tag{4.11}$$

Eliminating J from (4.10) and (4.11) and inverting the differentiation gives

$$x - x_0 = \int_0^\theta \frac{d\theta}{\{[1 - \beta(\cosh 2\theta - \sinh 2\theta) - \Delta' \sinh 2\theta]^2 + 4H^2\}^{1/2}} . \tag{4.12}$$

This integral can be inverted[6] in terms of elliptic functions. For the case with integrable solutions, $H = 0$, the result is simple. We have

$$\tanh\theta = \frac{g}{f} = \frac{1}{1+\beta}[(1-\bar{\beta}^2)^{1/2} + (\beta^2 - \bar{\beta}^2)^{1/2}] \times \tanh(1-\bar{\beta}^2)^{1/2}(x - x_0) , \tag{4.13}$$

where

$$\bar{\beta} \equiv [\beta^2 - (\kappa/x_0)^2]^{1/2} = [(2\beta - \Delta')\Delta']^{1/2} \approx (2\beta\Delta')^{1/2} .$$

The densities $f^2 - g^2 = J$ and $f^2 + g^2 = J\cosh 2\theta$ can now be obtained using (4.5) and (4.6). The "kink" in g/f is then given by $(1 \gg \beta \gg \Delta)$

$$\tanh\theta \approx (1 - \Delta')\tanh(x - x_0) \tag{4.14}$$

so that

$$\cosh 2\theta = \frac{1 + \tanh^2\theta}{1 - \tanh^2\theta} \xrightarrow[x\to\infty]{} 1/\Delta' .$$

We see that g/f should differ significantly from ± 1 only when $|x - x_0|$ is of order unity or smaller. Again, the typical solutions of Fig. 1 show this extreme localization of $1 - |g/f|$ very clearly.

V. DISCUSSION

The picture which has emerged from these classical solutions of the nonlinear spinor field is that of a thin ring, with thickness of the order of $1/\mu$, the bare mass of the fermion field. The mass is of the order 2ω, where ω represents the rotating mass. The radius of the ring is slightly larger than j/ω, where j is the orbital angular momentum. Thus the orbital velocity is of the order of $v/c \approx 1$. For large self-coupling ω/μ can be made arbitrarily small, but it increases as $\sqrt{j}$. Since the mass of the "bag" stemming from the nonlinear term remains proportional to the rotating mass, we find that the total mass increases proportionally to $\sqrt{j}$. We then obtain Regge trajectories, linear in the mass squared, at least up to angular momenta which keep $\omega/\mu \propto \sqrt{j}$ small. These soliton solutions are absolutely stable and represent classical concentrations of field, with some particle properties. Confined solutions in two-dimensional space-time of the four-fermion interaction have been presented in the literature lately,[5,7] and the question was raised of whether the four-dimensional version has similar solutions. In the two-dimensional problem, there is only one solution. What we have found here, however, is a much richer spectrum, consisting of linearly rising Regge trajectories of both parities, as well as daughters. This has considerable implications on what states should be considered "classical" and what states should be considered quantum excitations.

The relevance of classical solutions of nonlinear field equations to the quantum system have been studied extensively by various techniques.[8] In general, for renormalizable theories, the classical solutions can be considered a good starting point in considering quantum effects, at least in the weak-coupling limit.[9] For the nonlinear spinor field, some two-dimensional models have been considered semiclassically. In one case, where only one positive-energy state is allowed, there seems to be no correspondence between classical solutions and the mass spectrum found by the semiclassical method.[10] On the other hand, for the case which allows both positive- and negative-energy solutions,[7,10] the connection is complete. In four $(3+1)$ dimensions, the MacDowell symmetry relates solutions continued to negative energy with positive-energy solutions of opposite parity, and thus may have bearing on the question of the relevance of classical solutions to quantum systems.

ACKNOWLEDGMENTS

We wish to thank J. Watrous for his generous help in numerical calculations and to acknowledge the kind hospitality of the Aspen Center for Physics, where part of the work was done. One of us (P.K.) would like to thank Professor R. J. Finkelstein for very helpful discussions.

*Work supported in part by the National Science Foundation and the United States Energy Research and Development Administration.

[1] R. J. Finkelstein, R. Lelevier, and M. Ruderman, Phys. Rev. 83, 326 (1951); R. J. Finkelstein, C. Fronsdal, and P. Kaus, *ibid.* 103, 1511 (1956); D. Finkelstein

and C. W. Misner, Ann. Phys. (N.Y.) 6, 230 (1957); T. H. R. Skyrme, Proc. R. Soc. London A247, 260 (1958).

[2]Interest in solitons has been stimulated by monopole-type solutions in gauge theories. See for example H. B. Nielsen and P. Olesen, Nucl. Phys. B61, 45 (1973); L. Faddeev, Max-Planck-Institut (München) Report No. MPI-PAE/Pth16, 1974 (unpublished); G. 't Hooft, Nucl. Phys. B79, 276 (1976).

[3]S.-Y. Chu and P. Kaus, Phys. Rev. D 14, 1681 (1976).

[4]Much of the discussion of this section is contained in the second paper of Ref. 1.

[5]S.-J. Chang, S. D. Ellis, and B. W. Lee, Phys. Rev. D 11, 3572 (1975).

[6]The case $\kappa = 0$ ($\Delta = \beta$) is considered in P. Kaus, Phys. Rev. D 14, 1722 (1976). This case fully solves the two-dimensional (1+1) version as well as the asymptotic ($r \to \infty$) four-dimensional equations (Refs. 5, 7).

[7]S. Y. Lee, T. K. Kuo, and A. Gavrielides, Phys. Rev. D 12, 2249 (1975).

[8]For functional-integral techniques see R. F. Dashen, B. Hasslacher, and A. Neveu, Phys. Rev. D 10, 4114 (1974); 10, 4130 (1974); 11, 3424 (1975); J. L. Gervais and B. Sakita, *ibid.* 11, 2943 (1975); J. L. Gervais, A. Jevicki, and B. Sakita, *ibid.* 12, 1038 (1975); C. Callan and D. Gross, Nucl. Phys. B93, 29 (1975); L. D. Faddeev, IAS Report (unpublished).

For canonical quantization approach see N. H. Christ and T. D. Lee, Phys. Rev. D 12, 1606 (1975); E. Tomboulis, *ibid.* 12, 1678 (1975); M. Creutz, *ibid.* 12, 3126 (1975).

For variational techniques see W. A. Bardeen, M. S. Chanowitz, S. D. Drell, M. Weinstein, and T.-M. Yan, Phys. Rev. D 11, 1094 (1975). See also P. Vinciarelli, Lett. Nuovo Cimento 4, 905 (1972); M. Creutz, Phys. Rev. D 10, 1749 (1974); M. Creutz and K. S. Soh, *ibid.* 12, 443 (1975).

For Kerman-Klein method and Green's-function technique see J. Goldstone and R. Jackiw, Phys. Rev. D 11, 1486 (1975); A. Klein and F. R. Krejs, Univ. of Pennsylvania Report No. UPR-0039T, 1975 (unpublished); S.-J. Chang, Phys. Rev. D 12, 1071 (1975).

[9]See N. H. Christ and T. D. Lee, Ref. 8.

[10]S.-S. Shei, Phys. Rev. D 14, 535 (1976).

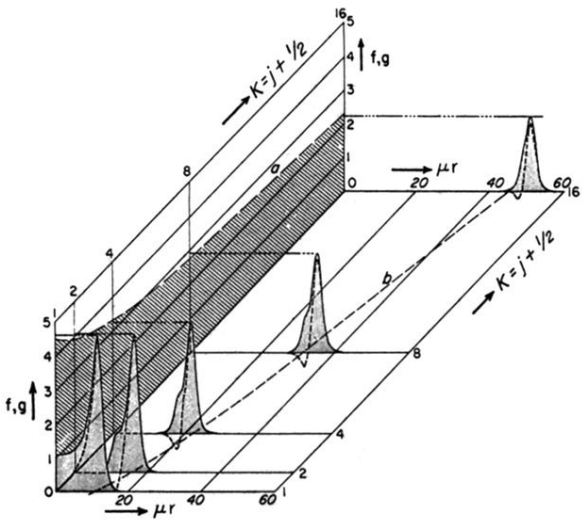

FIG. 4. Solutions f, g which correspond to the dimensionless coupling constant ($\gamma\mu^2 = 10^5$) for various $\kappa = j + \frac{1}{2}$ as functions of $x = \mu r$. The curves (a) $f = 4.7/\kappa^{1/4}$ and (b) $\mu r = 11\kappa^{1/2}$ are given for guidance. See text for significance of (a) and (b) as approximations for height and "radius" of solutions.